WIRE-MESH SENSORS FOR TWO-PHASE FLOW INVESTIGATIONS

Horst-Michael Prasser

1. Introduction

In the annual report 1996 a new wire-mesh sensor for gas-liquid flows was presented [1]. It was used to visualise the cavitation bubble behind a fast acting shut-off valve in a pipeline with a time resolution of over 1000 frames per second for the first time. In the last two years the sensor was applied to an air-water flow in a vertical pipeline (inner diameter D=51.2mm) to study the flow structure in a wide range of superficial velocities. Besides the void fraction distributions, the high resolution of the sensor allows to calculate bubble size distributions from the primary measuring data. It was possible to study the evolution of the bubble size distribution along the flow path with growing distance from the gas injection (inlet length, L).

2. Working principle of the wire-mesh sensor

The function is based on the measurement of the local instantaneous conductivity of the two-phase mixture. The sensor consists of two electrode grids with 16 electrodes each, placed at an axial distance of 1.5 mm behind each other. The conductivity is measured at the crossing points of the wires of the two grids. This results in 16x16 sensitive points, which are equally distributed over the cross section (Fig. 1). In the corners of the rectangular measuring grid some of the sensitive points lie outside the boundary of the circular cross section and cannot be used. Therefore, the number of points taking part in the measurement is 242. The wires have a diameter of 120 µm.

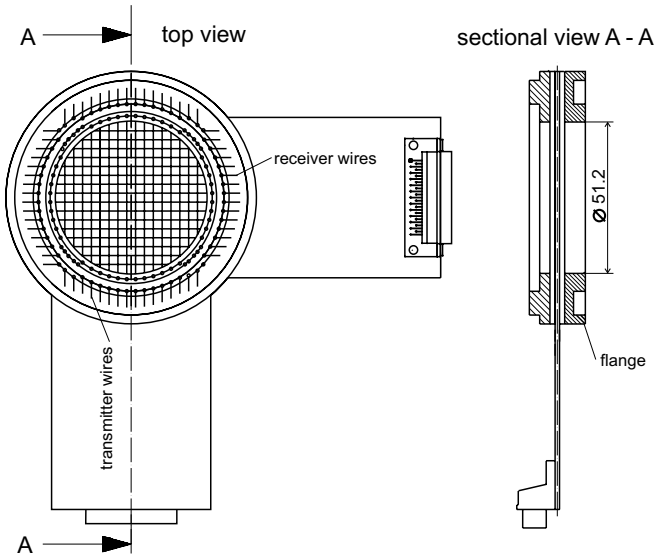

Fig. 1: Wire-mesh sensor (2 x 16 electrode wires)

For the conductivity measurement, one plane of electrode wires is used as transmitter, the other as receiver plane. During the measuring cycle, the transmitter electrodes are activated by a multiplex circuit in a successive order, as illustrated in Fig. 2 for an example of 2 x 4 wires. The time resolution achieved by the signal processing unit is 1200 frames per second. The spatial resolution is given by the pitch of the electrodes and equals 3 mm.

The measurement for one row is started by closing one of the switches S1-S4. The currents arriving at the receiver wires are transformed into voltages by operational amplifiers and sampled by individual sample/hold circuits. After an analogue/digital conversion the signals are recorded by a data acquisition computer and stored for each receiver electrode separately. This procedure is repeated for all transmitter electrodes.

During the activation of a single transmitter electrode all the other electrodes are kept on zero potential. This is done by low impedance input respectively output cascades (see Fig. 2). This special feature prevents a deterioration of the resolution by cross talk between parallel wires. In fact, the current from the activated wire flows towards all the other electrodes, but as the grounded wires cannot depart from zero potential there is no additional current from them to the given receiver wire. The network of grounded wires creates symmetry conditions, which prevent that the conductivity of the fluid far from the given crossing point can influence the locally measured value. In this way, the distribution of the electrical conductivity over the cross section occupied by the sensor is obtained row by row. After the last transmitter electrode has been activated, a two-dimensional matrix of 16 x 16 AD conversion results is available, which are proportional to the conductivity in the control volumes in the vicinity of all crossing points of two perpendicular wires. For more details about the signal acquisition see [2].

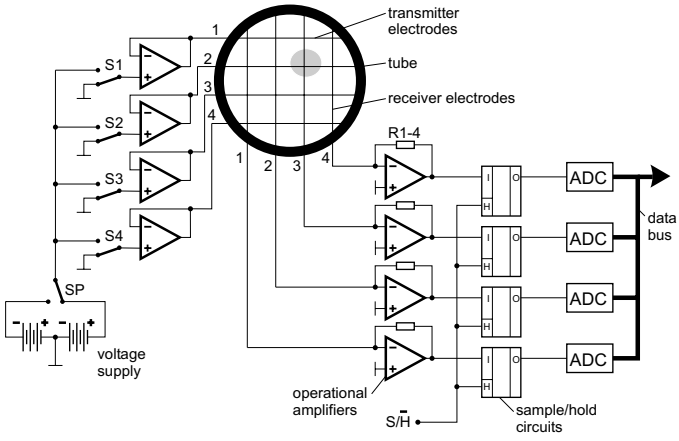

Fig. 2: Simplified scheme of a 2 x 4 wire-mesh sensor with signal acquisition system

3. Calculation of void fractions

During a calibration procedure, measurements for the situations "tube completely filled with liquid" and "tube completely filled with gas" are performed and the resulting matrices of AD conversion results are stored. The matrices acquired during the measurement of the two-phase flow are transformed into distributions of the void fraction by relating the individual measured components to the calibration values assuming a proportionality of local void fraction and electrical conductivity. The accuracy of the void fraction was tested by comparing line averages calculated from the wire-mesh data to the readings of a gamma-densitometer, which was located close to the wire-mesh sensor.

For that, the gamma-device (0.13 mCi Cs-137) was operated with an integration time of 120 s. This allowed to achieve a statistical accuracy of better than 1 %. The comparison to the gas fraction measured by the wire-mesh sensor is shown in Fig. 3. The dependency is linear within an error band of ± 5 % (related to the final value) in the following range of superficial velocities: J_{Air} 0.0024 - 12 m/s, J_{Water} 0.043 - 4 m/s.

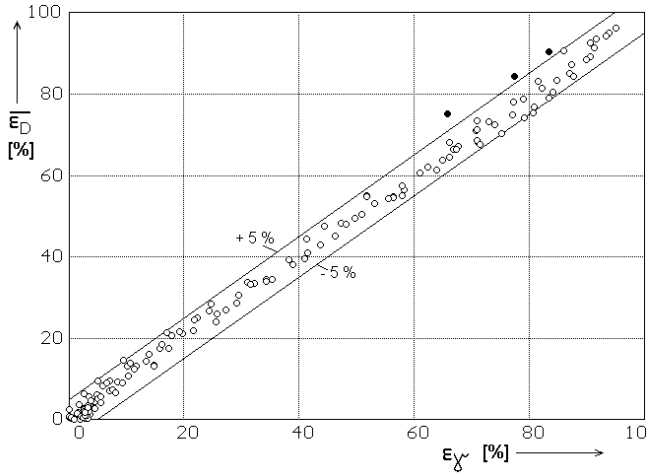

Fig. 3: Comparison between wire-mesh sensor and gamma-densitometer (black filled points: J_{Water}: 1.6 - 4 m/s; J_{Air}: 12 m/s)

4. Flow pattern visualisation

The output of the wire-mesh sensor consists of a time sequence of local instantaneous void fractions that characterise the presence of the gaseous phase in a grid of measuring positions in the cross section. These data sets can be used for a visualisation of the two-phase flow. With the help of a special software the individual gas fraction distributions can be displayed as a sequence of frames. Eulerian sectional views (pseudo side views) of the gas fraction distribution in the vertical center plane of the pipe can be obtained, if successive void fraction distributions over the diameter are plotted in a vertical stack, beginning from the top and moving downwards. When we assume that the gas bubbles travel with a constant velocity independently of their location in the cross section (radial velocity gradients are neglected), the phase velocity calculated from the average void fraction and the superficial gas velocity can be used to transform the time axis into a virtual z-axis.

Fig. 4 shows these sectional side views, obtained at different distances between air injection and wire-mesh sensor for a developed slug flow at J_{Water} = 1 m/s and J_{Air} = 0.48 m/s. The relation between horizontal and vertical dimensions of the bars in Fig. 4 are kept 1:1 with consideration the phase velocity of the gas, i.e. the shape of the gas bubbles, observed in the flow, is not distorted. In the presented experiment, the air was injected through 8 orifices in the wall of 4 mm diameter each. Therefore, the primary bubbles are therefore quite large. It has to be remarked that the side views represent a “frozen” flow pattern, characteristic for the given measuring position. In reality, the flow pattern continuously changes with growing height, e.g. at the sensor position of L = 30 mm above the injection we must expect the flow pattern of the next measuring position (L = 80 mm) at z=50 mm in the direction of the virtual z-axis, the flow pattern of the following position (L = 130 mm) at z=100mm, a.s.o..

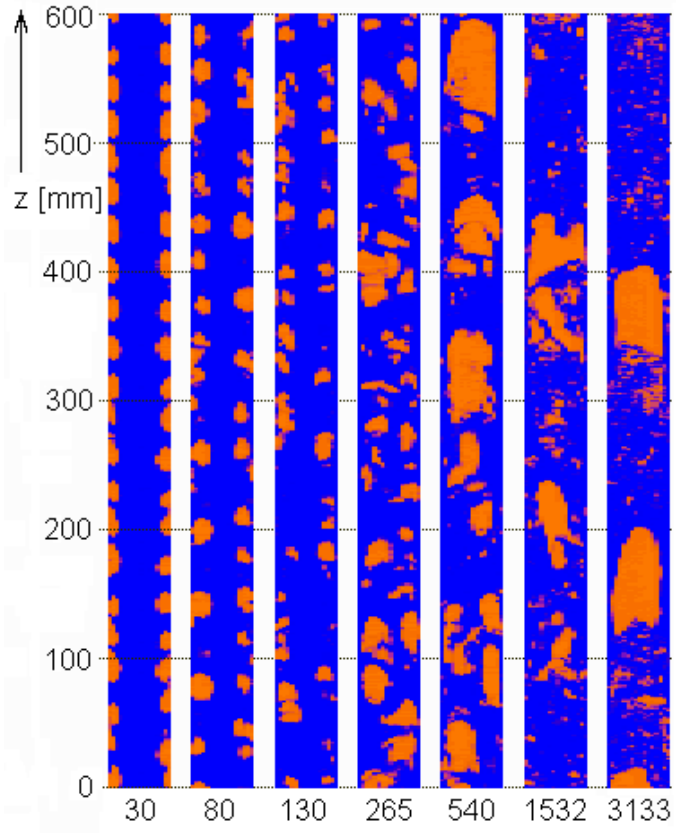

Fig. 4: Evolution of the flow pattern with growing distance from the air injection, J_{Water} = 1 m/s, J_{Air} = 0.48 m/s

The large primary bubbles are clearly visible at the distance of L = 30 mm. With growing height, they are more and more shifted towards the center of the pipe. Further, both coalescence and fragmentation occurs, leading to the appearance of bubbles either smaller or larger than the primary bubbles. In the end, slugs are formed. The characteristic shape of the slugs is very well reproduced by the sensor.

5. Bubble size distributions

The high spatial and time resolution of the wire-mesh sensor allows to calculate bubble size distributions from the measured gas fraction distribution sequence. After the transformation of the time axis into the virtual z-axis, described in the previous section, the measured data can be treated as a three-dimensional instantaneous void fraction distribution $\varepsilon_{x,y,z}$ with a resolution given by the pitch of the electrode wires ($\Delta x = \Delta y$ = 3 mm) in the x and y directions, and given by the phase velocity of the gas divided by the framing rate of f_{meas} = 1200 Hz in the z-direction (Δz = 1.4 mm in the example shown in Fig. 4). In the consequence, each bubble is mapped in several successive instantaneous void fraction distributions, delivered by the sensor (Fig. 5). The volume of an individual bubble V_{bub} can then be obtained by adding the local void fractions $\varepsilon_{x,y,z}$ of the grid points belonging to the selected bubble, multiplied by the magnitude of the control volume V:

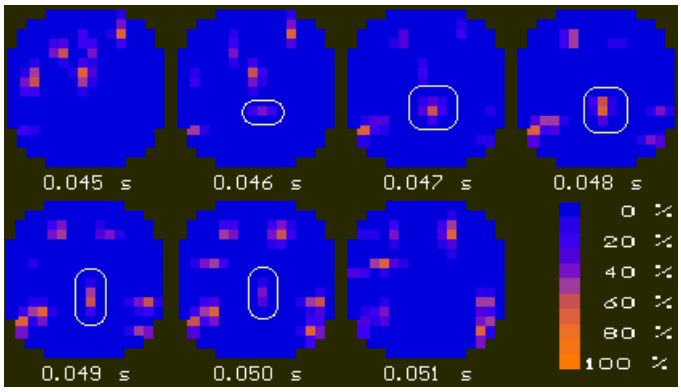

Fig. 5: Image of a selected bubble in a series of successive frames delivered by the sensor

$$V_{bub} = V \cdot \sum_{\varepsilon > \varepsilon_{min}} \varepsilon_{x,y,z} = \Delta x \cdot \Delta y \cdot \frac{J_{Air}}{\bar{\varepsilon}} \cdot \frac{1}{f_{meas}} \cdot \sum_{\varepsilon > \varepsilon_{min}} \varepsilon_{x,y,z} \qquad (1)$$

Here, the phase velocity of the gas is obtained from the superficial air velocity J_{Air} divided by the average void fraction $\bar{\varepsilon}$, which is determined by averaging the wire-mesh data. The summation is carried out by a recursive search procedure that starts at a grid position, where the void fraction is maximal. The summation must be terminated, when the boundary of the bubble is reached. Due to the presence of signal noise a termination threshold ε_{min} greater than zero must be defined. Otherwise, the recursive search could jump from one bubble to another via a channel of grid elements where the gas fraction is not accurately equal to zero. This would lead to an overestimation of the bubble volume. From the individual bubble volumes V_{bub}, equivalent bubble diameters D_{bub} were calculated:

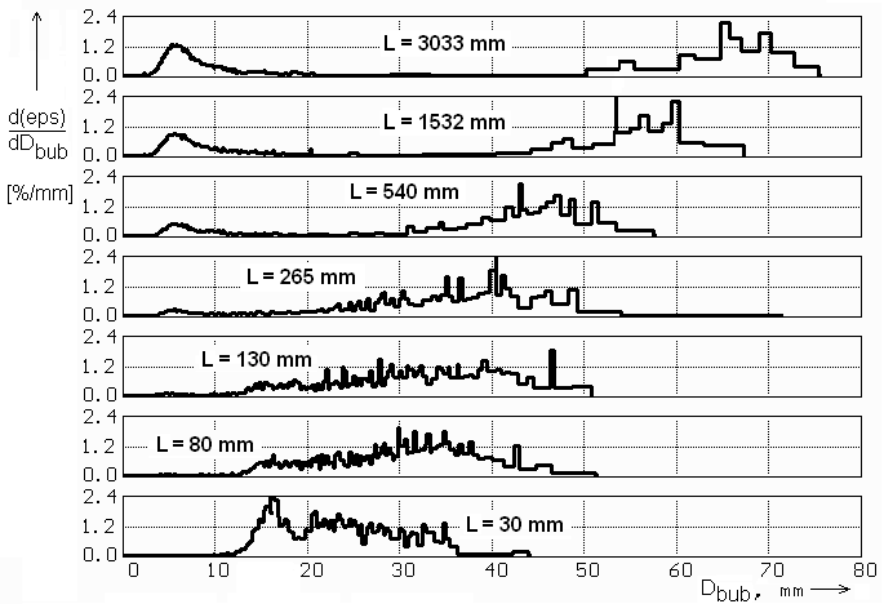

Fig. 6: Evolution of the bubble size distribution with growing distance L from the air injection, J_{Water} = 1 m/s, J_{Air} = 0.13 m/s

$$D_{bub} = \sqrt[3]{\frac{6}{\pi} \cdot V_{bub}} \qquad (2)$$

Bubble size distributions were constructed by summarising the contribution of the bubbles of a given range of diameters to the integral volumetric gas fraction. These partial void fractions are plotted against the equivalent bubble diameter. In Fig. 6 the evolution of the bubble size distribution at the flow conditions of Fig. 4 is shown.

At z = 30 mm the maximum of the bubble size distribution corresponds to the size of the primary bubbles (D_0). With growing height, the coalescence leads to the appearance of a second peak at a diameter of $\sqrt[3]{2} \cdot D_0$. These are bubbles that origin from coalescence between pairs of primary bubbles. At z = 1532 mm, a characteristic bimodal distribution is observed, which indicates the transition to slug flow. The large bubble fraction is still further developing with increasing height. At the same time, bubbles smaller than the primary bubbles appear due to fragmentation.

6. Void fraction profiles

When the instantaneous two-dimensional void fraction distributions are averaged over a long period, void fraction profiles can be obtained. Fig. 7 shows the development of the profiles at the superficial velocities of J_{Water} = 1 m/s, J_{Air} = 0.13 m/s for three different air injection conditions.

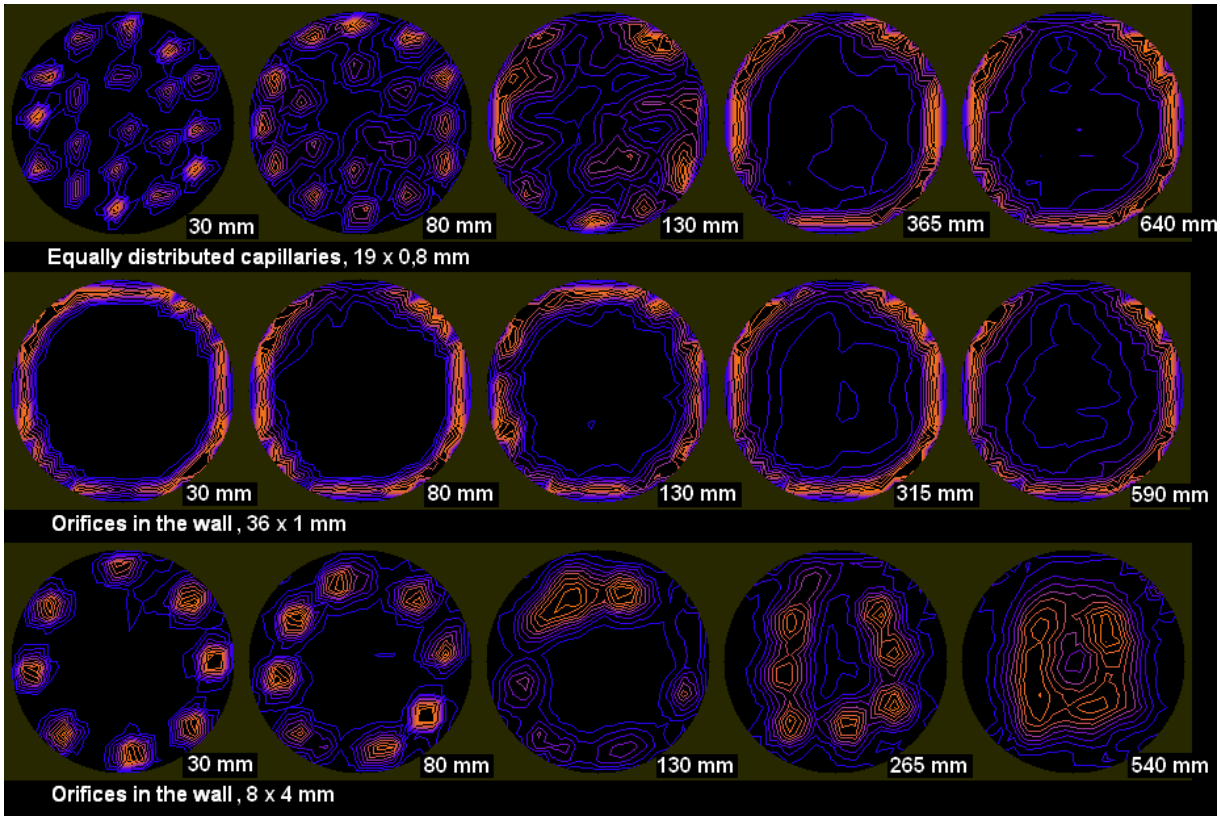

Fig. 7: Void fraction profiles averaged over 10 s for three different air injection conditions at different inlet length L, J_{Water} = 1 m/s, J_{Air} = 0.13 m/s

In case of 19 capillaries equally distributed over the cross section, at z = 30 mm a maximum of the void fraction is found at each individual position of an injecting capillary. With growing distance, the gas is pushed towards the wall by the lift force and a wall-peaked profile is formed. When the gas is injected through 36 orifices of 1 mm diameter, the peak at the wall is already formed by the mode of injection. A completely different behaviour is observed, when the gas is injected through large orifices of 4 mm diameter. Here, again each injecting orifice is visible in the void fraction distribution. But in contradiction to the injection by capillaries, the wall-peaking disappears with growing height, despite of the identical superficial velocities. The bubble size distributions are also significantly different even after a related inlet length of a approximately 60 L/D, as shown in Fig. 8.

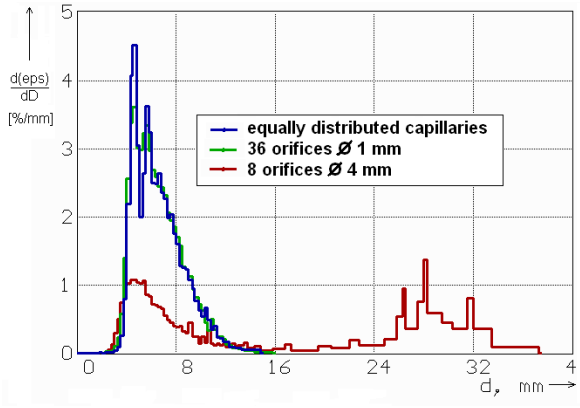

Fig. 8: Bubble size distributions at L ≅ 3100 mm (L/D ≅ 60) for three different air injection devices, J_{Water} = 1 m/s, J_{Air} = 0.13 m/s

7. Conclusion

The wire-mesh sensor provides detailed information about the structure of the two-phase flow. It is successfully used to visualise the air-water flow in a vertical pipeline. The comparison to gamma-densitometry has shown, that void fractions can be measured with good accuracy. From the primary measuring data it is possible to obtain void fraction profiles as well as bubble size distributions. Experiments were carried out to study the evolution of the flow structure with growing distance from the gas injection. A significant influence of the kind of the gas injection was found. The bubble size distributions clearly show the effect of coalescence and fragmentation. They can therefore be used for the development of bubble population models.

References

[1] H.-M. Prasser, A. Böttger, J. Zschau (1997), A New wire-mesh tomograph for gas-liquid flows, in F.-P. Weiß, U. Rindelhardt (Ed.), Annual Report 1996, Institute for Safety Research, FZR-190, 34-37

[2] H.-M. Prasser, A. Böttger, J. Zschau (1998), A new electrode-mesh tomograph for gas-liquid flows, Flow Measurement and Instrumentation 9, 111-119